




Cite this: *RSC Adv.*, 2019, 9, 16278

# Electrochemical immunosensor based on an antibody-hierarchical mesoporous SiO<sub>2</sub> for the detection of *Staphylococcus aureus*

Hongsu Wang, Yi Xiu,  Yan Chen, Liping Sun, Libin Yang, Honghao Chen and Xiaodi Niu\*

The outbreak of food-borne pathogens has become a serious concern; therefore, the detection of pathogenic bacteria in food is required. Untreated, sensitive, and reliable sensors should be developed for the detection of *Staphylococcus aureus* (*S. aureus*). In this study, a sensitive antibody-based electrochemical immunosensor was developed using antibody (Ab)-hierarchical mesoporous silica (HMS) bio-conjugates for label-free detection of low concentrations of *S. aureus*. First, a bio-template method based on butterfly wings was used to prepare the HMS. Then, the carrier material was amino-functionalized to cross-link the antibody with glutaraldehyde. The Ab-HMS bio-conjugates were then immobilized on a glassy carbon electrode (GCE), and the presence of *S. aureus* was detected by analyzing the changes in the peak currents after the antigen-antibody complex formation. Differential pulse voltammetry (DPV) was performed with bacterial concentrations ranging from 10 to  $2 \times 10^3$  colony forming units (CFU) mL<sup>-1</sup>. Selective tests were performed using *Escherichia coli* (*E. coli*), *Listeria monocytogenes* (*L. monocytogenes*), and *Salmonella*, and the selective assays showed specific detection of *S. aureus* using the sensor. In addition, the immunosensor showed a good linear relationship between the peak current increase and logarithmic *S. aureus* concentration ( $R^2 = 0.9759$ ) with a fast detection time (20 min) and detection limit of 11 CFU mL<sup>-1</sup>. When the electrochemical impedance spectroscopy (EIS) was performed under the same conditions, the results showed a good linear relationship between the impedance change value and the bacterial concentration ( $R^2 = 0.9720$ ), the limit of detection (LOD) was 12 CFU mL<sup>-1</sup>. The performance of the sensor was compared with that of the colony counting method in the spiked milk sample test. The results showed no significant difference in the test results. Hence, this electrochemical immunosensor can be used to quickly detect *S. aureus* in actual food samples with a high sensitivity, specificity and stability.

Received 2nd February 2019  
 Accepted 13th May 2019

DOI: 10.1039/c9ra00907h

rsc.li/rsc-advances

## 1. Introduction

*S. aureus* is an important zoonotic pathogen, belonging to the genus *Staphylococcus*, a conditional pathogen that is parasitic on the surface of the host. It can cause food contamination and bacteria as an important microbiological indicator in food. *S. aureus* is often detected in foods, such as frozen foods, animal foods, and vegetable products. According to reports, 20 ng of enterotoxin secreted by *S. aureus* in food can cause mild poisoning. The detection of *S. aureus* is achieved by detecting *Staphylococcus aureus* enterotoxin (SE). Only a few studies have been applied to detect the amount of *S. aureus* without pretreatment.<sup>1</sup> Therefore, a new method for detecting low concentrations of *S. aureus* is required.

For many years, conventional detection methods have included plate counting, fluorescence quantitative polymerase chain reactions,<sup>2</sup> enzyme-linked immunosorbent assays<sup>3</sup> and mediated isothermal amplification techniques.<sup>4</sup> These methods have been applied and approved; however, most methods are expensive and cannot meet the fast, accurate, and high-sensitivity requirements owing to the time and labor requirements.<sup>5</sup> Therefore, a rapid, convenient, and sensitive detection method for the quantitative detection of *S. aureus* concentration is required to prevent infection.<sup>6</sup>

Electrochemical biosensors have been increasingly used in detection methods owing to their specificity, sensitivity, rapidity, and reproducibility.<sup>7-9</sup> They are also regarded as important tools for monitoring and preventing pollution in food processing.<sup>10</sup> Because of the specificity of the antibody and the faster reaction time of the antigen and antibody, the antibody can be used as a detection substance to specifically detect *S. aureus*. To improve the sensor performance, mesoporous nanomaterials can be used.<sup>11,12</sup> Because of the high specific

College of Food Science and Engineering, Jilin University, Changchun 130062, People's Republic of China. E-mail: niuxd@jlu.edu.cn; Fax: +86-431-87836376; Tel: +86-431-87836376



surface area and large pore volume,<sup>13</sup> mesoporous nanomaterials are widely used in the fields of catalysis, medicine, and immobilization.<sup>14</sup> The bio-template strategy has provided a new method for the synthesis of mesoporous silica.<sup>15</sup> In recent years, functional nanomaterials have been prepared using bio-specific structures as templates.<sup>16</sup> It effectively utilizes a wide variety of biological materials found in nature and transforms them into mesoporous nanomaterials with functions and properties suitable for a wide range of applications in tissue engineering, drug delivery systems, photocatalysis, optics, and especially gas sensing.<sup>17</sup> Multi-stage pore nanomaterials can be widely produced by the biotemplate method,<sup>18</sup> such as cotton,<sup>19,20</sup> wood,<sup>21,22</sup> sponges<sup>23,24</sup> and butterfly wings.<sup>25</sup> In this experiment, HMS was synthesized using sol-gel methods to replicate the microstructure of butterfly wings.

There are already many detection techniques applied to the quantitative detection *S. aureus*. *S. aureus* was detected using a surface plasmon resonance biosensor with lysed phage as a specific and selective probe. Abbaspour *et al.*<sup>26</sup> developed an electrochemical immunosensor based on bis-aptamer to detect *S. aureus* with a detection limit of 1 CFU mL<sup>-1</sup>. Gómez *et al.*<sup>27</sup> produced an enzyme biosensor for the detection of *S. aureus* with a detection limit of 100 CFU mL<sup>-1</sup>. However, the prepared sensors are complicated in the production steps, are prone to waste materials that pollute the environment, and are rarely able to be quickly detected.

*S. aureus* is pathogenic, so the detection of *S. aureus* is imminent. HMS has suitable pore sizes and functional groups that can be covalently bound to antibodies to enhance shelf stability. Rapid and efficient detection of *S. aureus* can be achieved by using HMS to prepare biosensors. In this experiment, the microscopic porous structure of butterfly (*Papilio maackii*) wings was replicated using the sol-gel method. The structure, morphology, and chemical composition of the prepared nanomaterials were characterized by various analytical techniques. Then, a chemical modification was used to bind the antibodies to the HMS. Specifically, the amino group was functionalized, and then, the antibody was cross-linked with glutaraldehyde to immobilize the antibody. The immobilized material was fixed

on the surface of the GCE, and different concentrations of *S. aureus* were detected by DPV and EIS.<sup>28-30</sup> The sensor is not only simple to manufacture, but also has a fast detection time and can detect *S. aureus* with low sensitivity, and the sensor has a long shelf life. The sensor concept is shown in Scheme 1.

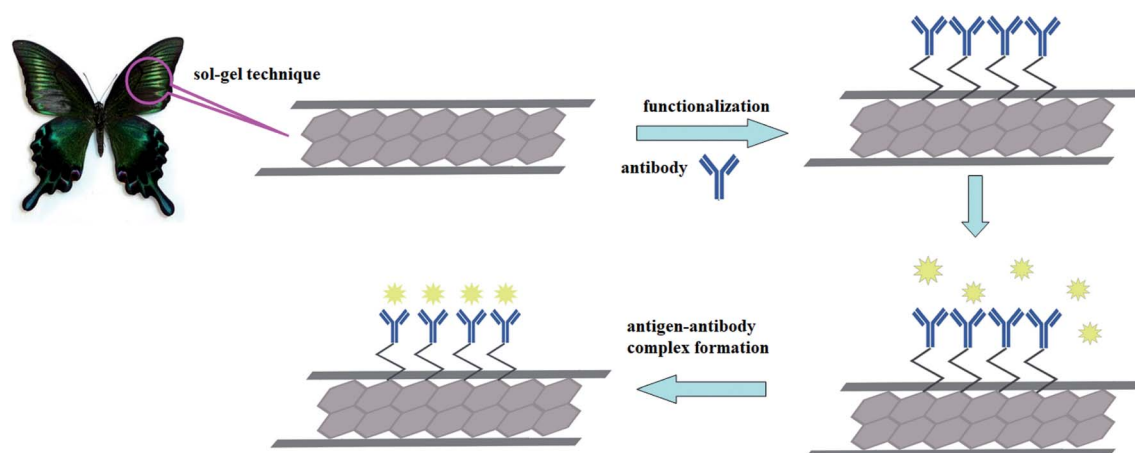
## 2. Experimental section

### 2.1. Materials

The butterfly species was *Papilio maackii* and was purchased from Beijing Jiaying Art Insect Museum. Hydrochloric acid (HCl), sodium hydroxide (NaOH), potassium hexacyano ferrate (K<sub>3</sub>[Fe(CN)<sub>6</sub>]), potassium chloride (KCl), toluene solution, titanium *n*-butoxide (TBT), cetyltrimethylammonium bromide (CTAB), absolute ethanol, tetraethyl orthosilicate (TEOS), glutaraldehyde (50%), dimethylformamide (DMF), tween solution, and PBS buffer solution (1×, pH 7.4) were purchased from Beijing Chemical Factory Reagents Company. 3-Aminopropyltriethoxysilane (98%) (APTES) was purchased from Alfa Aesar. For analytical purity, distilled water was used. *S. aureus*, *E. coli*, and *L. monocytogenes* were provided by the College of Animal Medicine, Jilin University. Rabbit anti-*Staphylococcus aureus* antibody (polyclonal antibody; ab20920) was purchased from Abcam (UK).

### 2.2. Apparatus

The morphology and structure of the HMS were determined by scanning electron microscopy (SEM; JEOL Hitachi S-4800, Japan) and transmission electron microscopy (TEM; FEI Tecnai G2F30). The surface functional groups of the HMS were measured by Fourier-transform infrared (FTIR) spectroscopy (Shimadzu IR Prestige-21) using the conventional KBr pellet technique and X-ray photoelectron spectroscopy (XPS; SSI S-ProbeX). N<sub>2</sub> adsorption-desorption isotherms were measured using a Micromeritics ASAP 2020 analyzer. Electrochemical experiments were carried out using a Chenhua CHI660E electrochemical workstation (CH Instruments, Shanghai, China). All electrochemical tests were recorded using a conventional



**Scheme 1** Schematic illustration of the preparation of electrochemical immunosensor based on an Ab-HMS materials.



three-electrode system, where a GCE, Ag/AgCl (3 M KCl) electrode, and Pt wire electrode were used as the working electrode, reference electrode, and counter electrode, respectively.

### 2.3. Bacterial cultivation

*S. aureus*, *E. coli*, *L. monocytogenes*, and *Salmonella* were respectively cultured in an LB broth medium at 37 °C for 12 h in an incubator at 150 rpm. The optical density of the cultured bacteria was obtained at 600 nm using a UV-Vis spectrophotometer. Then, each enriched bacterial strain was centrifuged at 5000 rpm for 5 min at 25 °C. The supernatant was discarded, and a gradient was diluted with sterile PBS (0.1 M, pH = 7.4). Each step of this process was performed under aseptic conditions.

### 2.4. Preparation of HMS and chemical modification

HMS was prepared by a surface sol-gel method using butterfly wings as a biological template and according to previous research methods. First, the butterfly wing specimens were dried, immersed in a 7.4% HCl solution for 4 h at room temperature, washed with distilled water, and dried at 80 °C. Then, the sample was immersed in a 6% NaOH solution at 60 °C for 3 h, washed with distilled water, and dried at 80 °C. The pretreated sample was immersed in an appropriate amount of TBT solution (100 mM titanium *n*-butoxide in 1 : 1 toluene-ethanol (v/v)) to fix the butterfly shape, soaked for 20 min each time, rinsed with absolute ethanol and distilled water, and dried at 80 °C, repeating 3 times. At room temperature, 0.25 g CTAB was added into a mixture of 40 mL ethanol and 30 mL

water, and the solution was stirred for approximately 30 min. Here, 150 mg of the treated samples were added to the mixture and stirred at room temperature for 1 h. After an ultrasonication treatment for 30 min, 120  $\mu$ L of 1 M NaOH solution was injected into the mixture under stirring. Then, 0.5 mL TEOS was added dropwise to the mixture under vigorous stirring at room temperature. After stirring for 12 h, the sample was filtered, washed with water, and dried at 30 °C overnight. The prepared sample was calcined in air at 600 °C for 5 h to obtain a white powder, which was HMS.

Here, 0.5 g of HMS was weighed. Then, 50 mL of anhydrous toluene and excess APTES were added, and the mixture was refluxed at 120 °C for 16 h and cooled to room temperature. The powder was collected by filtration and then extracted with an ethanol extractor for 24 h to obtain HMS with amino groups (NH<sub>2</sub>-HMS).

Next, 0.2 g of NH<sub>2</sub>-HMS was dispersed in 30 mL of absolute ethanol, and 0.2 g of 50% glutaraldehyde was added and stirred at room temperature for 12 h. The solid samples were washed repeatedly, filtered with absolute ethanol, and dried in an oven to obtain NH<sub>2</sub>-HMS with aldehyde groups (A-NH<sub>2</sub>-HMS).

### 2.5. Combination of the antibody to HMS

2 mg of A-NH<sub>2</sub>-HMS were dispersed in 2 mL of DMF solution, sonicated for 2 h, and centrifuged at 5000 rpm for 30 min. The supernatant was removed, and 10  $\mu$ L of the antibody were added. The reaction was carried out for 2 h at room temperature. After centrifugation at 15 000 rpm for 10 min, the supernatant was discarded, and 1 mL of Tween-20 was added. The Ab-HMS bio-conjugate was vortexed and stored at 4 °C.

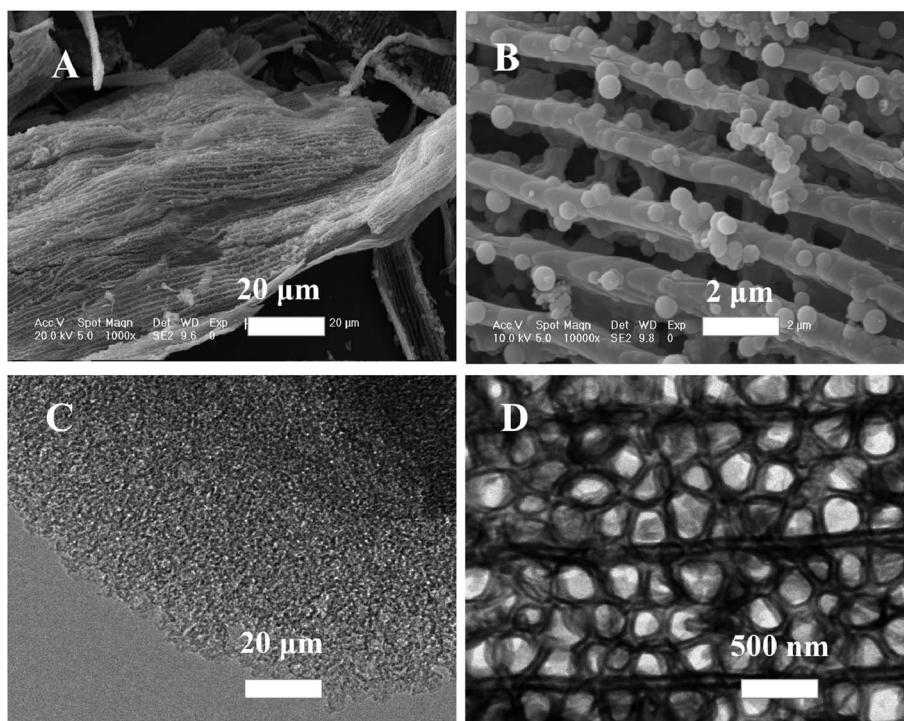


Fig. 1 (A and B) Scanning electron micrographs and (C and D) transmission electron micrographs of synthesized HMS.



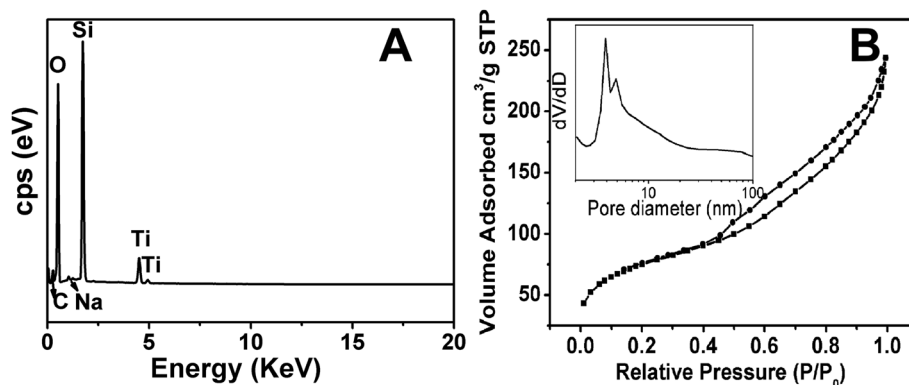


Fig. 2 Energy dispersive spectrometer (EDS) pattern of HMS (A) and nitrogen adsorption–desorption isotherm loop of HMS microspheres (B). The inset of (B) shows the pore-size distribution calculated from the desorption branch by the BJH model.

## 2.6. Preparation of electrochemical immunosensor

4  $\mu\text{L}$  of the Ab-HMS bio-conjugate was dropped onto the surface of the GCE and incubated at room temperature for 20 min. The unbound antibody was washed off with PBS and dried at room temperature. Then, 4  $\mu\text{L}$  of different concentrations of *S. aureus* PBS suspension were dropped onto the surface of the electrode at room temperature for 20 min. For the selectivity studies, the electrode was incubated with *E. coli*, *L. monocytogenes*, and *Salmonella* following the same protocol as that for *S. aureus*.

## 2.7. Electrochemical characterization

DPV, electrochemical impedance spectroscopy (EIS) and cyclic voltammetry (CV) were performed using Autolab, potentiostat/galvanostat, and NOVA 1.10 software (Metrohm, Netherlands). All electrochemical measurements were performed at room temperature using 10 mM PBS containing 1 mM  $[\text{Fe}(\text{CN})_6]^{3-/4-}$  and 0.1 M KCl. DPV, EIS and CV were performed for the electrochemical characterization of GCE, HMS-GCE, and Ab-HMS-GCE. All calculations and analyses were performed using Origin 8.51 software.

# 3. Results and discussion

## 3.1. Physical characterization of HMS

As shown in Fig. 1A, at a lower magnification, the sample had a sheet-like morphology, and the organic ridges of the butterfly wings were visible on each sample of the sheet. The morphology distribution of each sheet sample was similar and uniform, which proved that the synthesis method used in this study improved the success rate. In the high magnification image (Fig. 1B), the structure of the scale surface of the butterfly wing was visible. The organic ridges were extended in parallel, and the structure between the ridges was porous. A circular hole having a diameter of approximately 1  $\mu\text{m}$  was formed by the organic texture; therefore, the structure between the organic ridges looked like a network. The distance between the two

parallel ridges was approximately 1  $\mu\text{m}$ . The original shape of the butterfly wing was fixed during the synthesis process. Thus, the spine did not break, and it was a complete structure.

TEM can effectively detect the type and structure of mesoporous material. From the TEM image (Fig. 1C and D), the morphological structure and scanning electron micrograph showed the same subtle structure.<sup>31</sup> The complete structure of the silica replica is shown at a low magnification, and the dark and dense portion is the replica of the butterfly wing cylindrical structure. The thin area between the obsessive walls is a replica of the cellular tissue, and at a higher magnification, this replication structure is more visible.

From the spectrum analysis (Fig. 2A), the material contained a large amount of O and Si elements, demonstrating that the material was a silica component. The titanium *n*-butoxide reagent was used to fix the butterfly wing morphology. Therefore, it contained a small amount of Ti elements. The trace amounts of C and Na elements could be owing to reagent washout and calcination; however, they had no effect on the experiment. The percentage of each element is known by EDS characterization and is listed in Table 1. It can be seen that the proportion of Si element and O element is the highest.

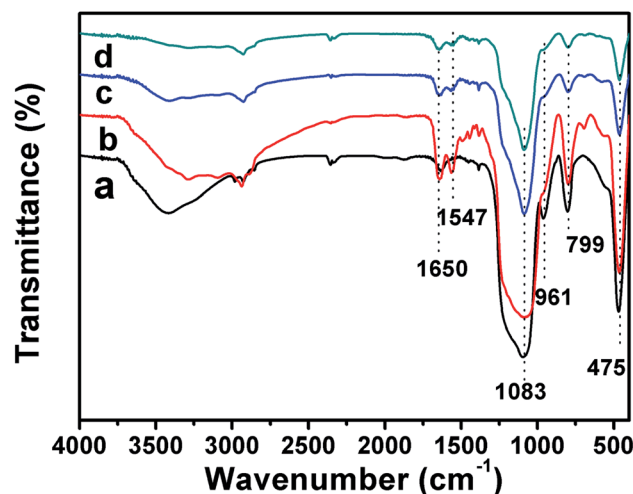


Fig. 3 Fourier-transform infrared (FT-IR) spectra of (a) HMS, (b)  $\text{NH}_2$ -HMS, (c) A- $\text{NH}_2$ -HMS and (d) Ab-HMS.

Table 1 Percentage of composition of each component in HMS (%)

Element	C	O	Na	Si	Ti
Atomic percentage (%)	13.59	64.57	0.46	17.76	17.76



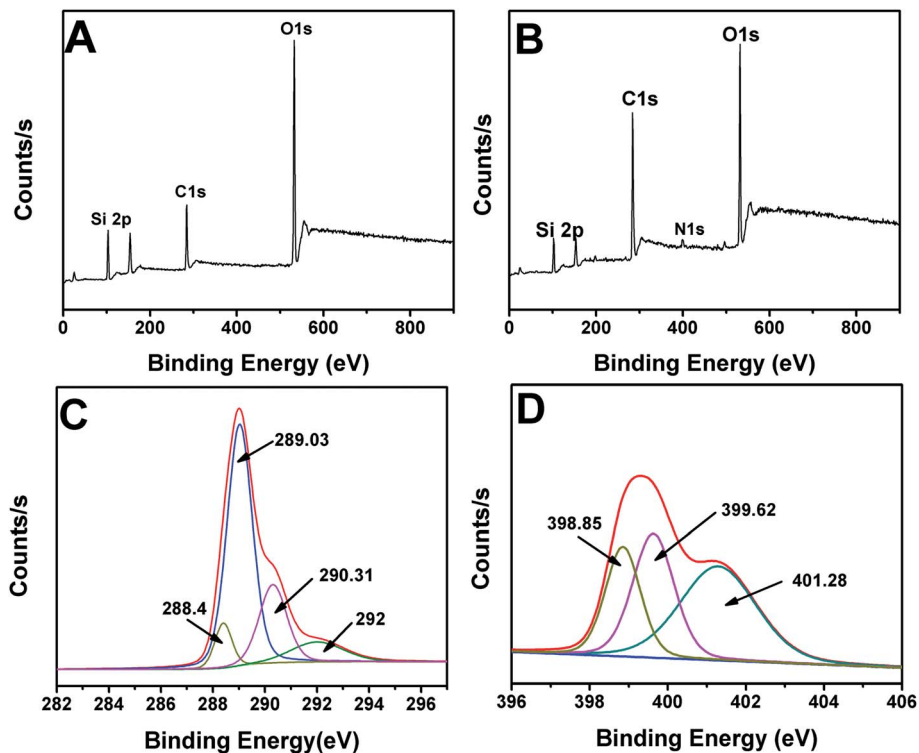


Fig. 4 The X-ray photoelectron spectrum (XPS) of HMS (A), Ab-HMS (B), C 1s (C) and N 1s (D) spectra of Ab-HMS.

As shown in Fig. 2B, the nitrogen adsorption–desorption isotherm curve of HMS belonged to the type IV isotherm.<sup>32</sup> The isotherms all corresponded to capillary condensation at a  $p/p_0$  value of approximately 0.43. A distinct H1 hysteresis loop appeared between 0.43–1.0, which indicated that the pore size of the HMS was uniform, and the permeability of the mesopores was good.<sup>33</sup> When the  $p/p_0$  value was small, single/multilayer adsorption occurred inside the pores, and the gas adsorption amount increased slowly. As the  $p/p_0$  value increased, the gas adsorption amount rapidly increased, and gas multi-layer adsorption occurred in the material. The HMS had a specific surface area of  $257.0213 \text{ m}^2 \text{ g}^{-1}$ , a pore diameter of 1.03 nm, and a pore volume of  $0.33 \text{ cm}^3 \text{ g}^{-1}$ . The material had a mesoporous structure.<sup>34</sup>

Fig. 3 shows the change in the group during the binding of the carrier material to the antibody (recorded in the range of  $4000 \text{ cm}^{-1}$  to  $500 \text{ cm}^{-1}$ ). In spectrum (a), the strong and broad absorption band at  $1083 \text{ cm}^{-1}$  indicates the antisymmetric absorption vibration of Si–O–Si.<sup>35,36</sup> The peaks at  $475 \text{ cm}^{-1}$  and  $799 \text{ cm}^{-1}$  are caused by the bending vibration and symmetric stretching vibration of Si–O–Si, respectively. The absorption band at  $961 \text{ cm}^{-1}$  is attributed to the bending vibration of Si–OH. These are characteristic absorption peaks of silica and proved that there were hydroxyl groups on the surface of the HMS, allowing the possibility of subsequent group modification.<sup>36</sup> In spectrum (b), the absorption peaks at  $1547 \text{ cm}^{-1}$  and  $1650 \text{ cm}^{-1}$  are owing to the C=N stretching vibration, thereby demonstrating that amino groups were successfully grafted on

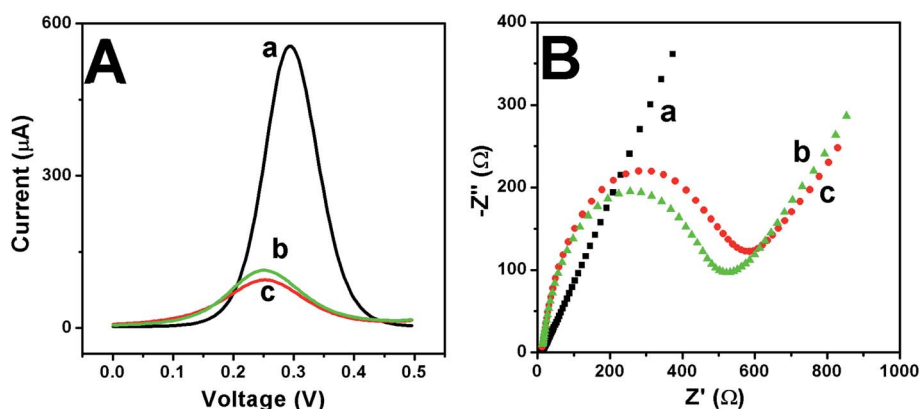


Fig. 5 DPV (A) and EIS (B) in the presence of  $1 \text{ mM } [\text{Fe}(\text{CN})_6]^{3-/4-}$  as the redox medium for characterization of GCE (a), HMS-GCE (b) and Ab-HMS-GCE (c).



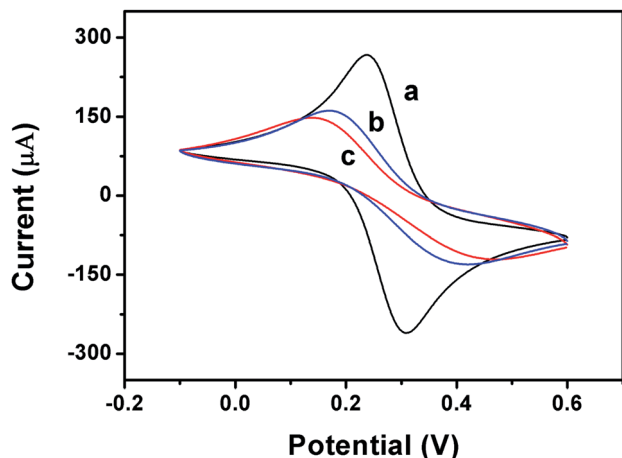


Fig. 6 CV in the presence of 1 mM  $[\text{Fe}(\text{CN})_6]^{3-/4-}$  as the redox medium for characterization of GCE (a), HMS-GCE (b) and Ab-HMS-GCE (c).

the surface of the HMS. For spectrum (c), the absorption peak at  $1650\text{ cm}^{-1}$  gradually narrowed and weakened, and the disappearance of the absorption band at  $1547\text{ cm}^{-1}$  was owing to the grafting of the glutaraldehyde aldehyde group and amino bond reaction. In spectrum (d), the same phenomenon as that in spectrum (c) was shown, because the grafted aldehyde group was chemically bonded to the amino group on the antibody, indicating that the antibody was successfully immobilized on the HMS.<sup>37</sup>

Fig. 4 shows the elemental composition of HMS and Ab-HMS and the electronic states of the elements. HMS mainly contains Si, C, and O elements, which is the same as the EDX characterization. It can be seen from Fig. 4B that Ab-HMS contains not only three elements of Si, C, and O but also an element of N, since the bound antibody has an amino group, thereby introducing an N element. Fig. 4C shows the energy spectrum of C 1s in Ab-HMS. The high-resolution peaks are 288.4, 289.03, 290.31, and 292 eV, respectively, corresponding to the forms of  $-\text{C}=\text{O}$ , C-O, C-Si, and C-Na. In Fig. 4B, the peak at 398.85 eV originates from the nitrogen atom in the  $\text{sp}^3$  configuration, and the peak at 399.62 eV originates from  $\text{sp}^2$ , which corresponds to the amide bond. And the peak at 401.28 eV is attributed to the presence of  $-\text{NH}_2$ . It can be proved that the antibody and the mesoporous

material are covalently bonded through the amide bond, thereby improving the stability of the immobilization.<sup>38,39</sup>

### 3.2. Functionalized electrode characterization

An electrochemical characterization was performed using DPV and EIS with  $\text{K}_3[\text{Fe}(\text{CN})_6]$  as the electron transfer medium. As shown in Fig. 5A, the polished GCE had a peak current value of  $500\text{ }\mu\text{A}$ . When the HMS was added, the surface of the electrode was not smooth. Thus, the peak current value dropped significantly, and when the Ab-HMS bio-conjugate was added to the electrode surface, the peak current value decreased again. Because the electron transfer behavior was blocked after the antibody was immobilized, the current value decreased again. The impedance measurement results were in good agreement with the DPV measurement results. The impedance value is represented by the diameter of the measurement circle. From Fig. 5B, the impedance spectrum of the bare GCE is a straight line,<sup>40</sup> and the impedance value of the HMS-GCE is less than that of Ab-HMS-GCE.

In order to more fully demonstrate that the conjugate was successfully immobilized on the GCE surface, GCE, HMS-GCE and Ab-HMS-GCE were subjected to cyclic voltammetry (CV) to detect electrical signals. As shown in Fig. 6, GCE had a pair of obvious in solution. The redox peak, while HMS-GCE due to the low conductivity of silica, the redox peak is not as clear as the bare electrode. After the immobilization of the antibody, the redox peak is most pronounced, which is consistent with the results of DPV and EIS. Fig. 7 shows CV of the biosensor at a scan speed of 10, 50, 100, 150, 200  $\text{mV s}^{-1}$ . It can be seen from Fig. 7A that the peak current of the sensor increases as the scanning speed increases. Fig. 7B shows that the peak current value is linear with the square root of the scan speed, and the correlation coefficients are all greater than 0.99. It is demonstrated that the working electrode has an electrocatalytic behavior and the electron transfer process of the surface is controlled to diffuse diffusion, thereby providing sufficient electron accessibility to shuttle between the antibody and the electrode.<sup>8,11</sup>

### 3.3. Experimental conditions optimization

As shown in Fig. 8A, when the incubation time was 20 min, the response current of the sensor reached its maximum value, and

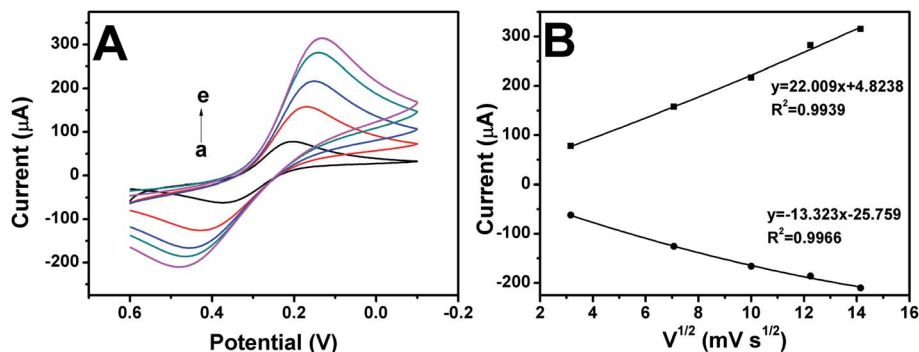


Fig. 7 (A) CV of Ab-HMS-GCE at different scanning speeds of 10 (a), 50 (b), 100 (c), 150 (d), 200 (e)  $\text{mV s}^{-1}$  in 1 mM  $[\text{Fe}(\text{CN})_6]^{3-/4-}$  and (B) the linear relationship between the square root of the scanning speed and the peak current.



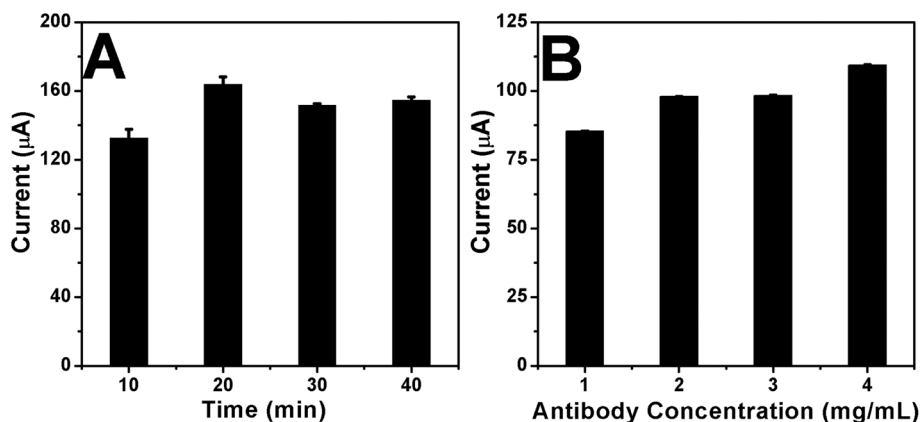


Fig. 8 (A) Response time studies for interaction of *S. aureus* with Ab-HMS-GCE modified surface and (B) study on the interaction between *S. aureus* and different antibody concentrations.

as time increased, the current value decreased slightly. This could be because of the excessive exposure to air, which created other substances on the surface of the electrode, reducing the electrode sensitivity and response current. As shown in Fig. 8B, when the antibody concentration reached 4 mg mL<sup>-1</sup>, the response current of the sensor reached the maximum value. Therefore, when the *S. aureus* test was performed, the concentration of the loaded antibody was 4 mg mL<sup>-1</sup>.

### 3.4. Differential pulse voltammogram of *S. aureus* detection

In Fig. 9, when the concentration of bacteria was in the range of 10 to 2 × 10<sup>5</sup> CFU mL<sup>-1</sup>, a linear relationship between the peak current and logarithmic *S. aureus* concentration was observed, and the correlation coefficient  $R^2$  was 0.9759. The limits of detection (LOD) was calculated according to the signal-to-noise ratio method. The coefficient was 3, and the standard deviation was 0.005 in blank PBS. The LOD was 11 CFU mL<sup>-1</sup>, which is more sensitive than that of previous studies. Neha Bhardwaj *et al.* developed an MOF-based

phage sensor for the detection of *S. aureus* with a detection limit of 31 CFU mL<sup>-1</sup>.<sup>41</sup> Ward *et al.* used screen-printed carbon electrodes to detect *S. aureus*, and the lowest detection concentration was 1.8 × 10<sup>6</sup> CFU mL<sup>-1</sup>,<sup>42</sup> which was higher than the minimum detection concentration of the sensor designed in this study.

DPV was used to detect the concentration of *S. aureus*. As shown in Fig. 9, as the concentration increased, the peak current value also increased. According to previous reports,<sup>43</sup> the reason for the increase of current with increase in the concentration of bacteria could be the conformational change of the cells and the antigen-antibody complex formed during the binding process could cause the current increase, which cause changes in the electrode's surface conductivity. Because bacterial electrochemical reactions are produced exclusively by extracellular electrons, when the droplets of the bacteria are on the surface of the electrode, the antigen specifically reacts with the antibody, and the contents of the cells flow out, including some electrolytes and conductive metal ions that are deposited on the surface of the electrode. This enhances the conductivity

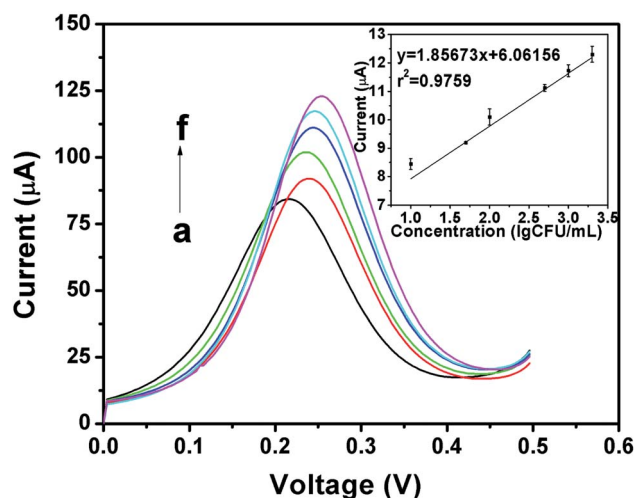


Fig. 9 Sensitivity of the immunosensors. DPVs of varying concentration of *S. aureus* from 10 to 2 × 10<sup>5</sup> CFU mL<sup>-1</sup> (from a to f) in PBS (1×, pH 7.4) containing 1 mM [Fe(CN)<sub>6</sub>]<sup>3-/4-</sup> and 0.1 M KCl in PBS. Inset: corresponding calibration plots of peak current versus concentration of *S. aureus* detection.

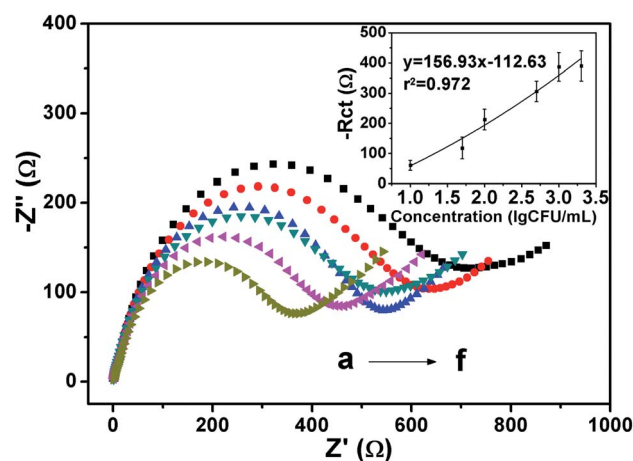


Fig. 10 Sensitivity of the immunosensors. EISs of varying concentration of *S. aureus* from 10 to 2 × 10<sup>5</sup> CFU mL<sup>-1</sup> (from a to f) in PBS (1×, pH 7.4) containing 1 mM [Fe(CN)<sub>6</sub>]<sup>3-/4-</sup> and 0.1 M KCl in PBS. Inset: corresponding resistance difference and calibration curve for *S. aureus* detection concentration.



Table 2 Comparison of reported biosensors with present work

Purposed biosensor	Detection method	Linear range (CFU mL <sup>-1</sup> )	LOD (CFU mL <sup>-1</sup> )	Ref.
Potentiometric biosensor	Potentiometric titration	$2.3 \times 10^3$ to $2 \times 10^4$	800	46
Colorimetric biosensor	Colorimetry	75 to $7.5 \times 10^6$	40	47
Electrochemiluminescent biosensor	Electrochemiluminescent	$1.0 \times 10^3$ to $1.0 \times 10^9$	$3.1 \times 10^2$	48
MOF-bacteriophage biosensor	Immunofluorescence	40 to $4 \times 10^8$	31	41
Impedimetric biosensor	EIS	$10^2$ to $10^6$	100	49
Electrochemical immunosensor biosensor	DPV	10 to $2 \times 10^3$	11	This work

of the whole cell and causes an increase in the electrochemical peak current with an increasing *S. aureus* concentration.<sup>25</sup> The larger specific surface area of the nano-mesoporous material loads more antibodies, which makes the reaction more thorough. When the potential is increased during the electrochemical detection process, the surrounding environment becomes unfavorable to the cells, and teichoic acid in the cell wall will start to accumulate cations in the PBS solution,<sup>44</sup> including hydrogen ions. Therefore, the conductivity will increase, and the hydrogen ions will affect the pH of the solution. Because the pH also affects the peak position during the detection process, different concentrations of bacteria will have slightly different peak positions during DPV detection.<sup>45</sup> In order to verify the accuracy of the reaction mechanism of this experiment, EIS detection method was used to quantitatively detect *S. aureus* under the same conditions. As shown in the Fig. 10, as the concentration of bacteria increased, the electron transport ability of the electrode surface increased. Therefore, the electrode resistance is reduced. There is a good linear relationship between the resistance difference and the bacterial concentration ( $R^2 = 0.9720$ ), the LOD is  $12 \text{ CFU mL}^{-1}$  ( $S/N = 3$ ) which is consistent with the DPV detection trend, so the experimental principle of the experiment is proved to be accurate, and the sensor can be applied to the quantitative detection experiment of *S. aureus*.<sup>29,30</sup> Table 2 lists the detection results of several *S. aureus* biosensors. The sensors designed in this study were superior to the other detection methods in terms of the detection range and detection limit.

### 3.5. Direct measurement of *S. aureus* in whole milk

To evaluate the performance of the sensor in food, the bacterial concentration in the same milk sample was detected by the colony counting method and sensor, and the test results are listed in Table 3. The biosensor measurement results were not significantly different from those measured by the plate count method, indicating that the sensor could be applied to actual sample detection. The conventional flat panel counting method has a long operation time and cumbersome processing steps. In contrast, the sensors designed in this study do not require pre-processing and are quick and easy to operate. Therefore, the sensors can be applied to other actual sample inspections.

### 3.6. Specificity determination

The PBS of different bacteria (*E. coli*, *L. monocytogenes*, and *Salmonella*) was added to the surface of the sensor to test the specificity at a concentration of  $10^2 \text{ CFU mL}^{-1}$ . As shown in

Fig. 11, the current change of *S. aureus* was larger than that of other bacteria of the same concentration, indicating that the sensor had a good specificity for *S. aureus*.

### 3.7. Stability test

The prepared working electrode was stored at 4 °C when not use. *S. aureus* ( $2 \times 10^3 \text{ CFU mL}^{-1}$ ) was used to study the stability of the sensor for 15 days. No significant change in current was observed after 5 days of storage. The relative standard deviation was 0.54%, retaining 90.09% of the initial current. After 10 days of storage, the relative standard deviation was 0.91%, retaining 84.47% of the initial current. After 15 days, the relative standard deviation was 2.19%, and 81.41% of the initial current was retained. Based on these stability data, we can conclude that the biosensor prepared in this experiment has good stability.

Table 3 *S. aureus* determination by plate counting and Ab-HMS-GCE sensor<sup>a</sup>

Whole milk sample	Spike (CFU mL <sup>-1</sup> )	Measured value (CFU mL <sup>-1</sup> )	Spiked recovery (%)
1	42	$38 \pm 0.02$	90%
2	144	$132 \pm 0.08$	92%
3	240	$234 \pm 0.08$	97%
4	1102	$1122 \pm 0.21$	102%

<sup>a</sup> Data expressed as mean  $\pm$  standard deviation (average of three replications for *S. aureus*).

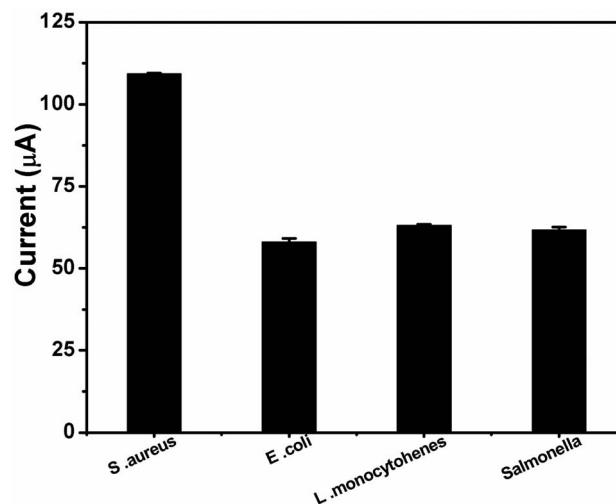


Fig. 11 Histogram depicting the selectivity of immunosensors for *S. aureus*, *E. coli*, *L. monocytogenes* and *Salmonella*.





## 4. Conclusions

In this study, a sensitive electrochemical immunosensor for label-free *S. aureus* detection was developed using antibodies covalently bound to HMS. The preparation of HMS by the biological template method could successfully replicate the multi-stage pore structure of butterfly wings and protect the environment without generating other waste materials. Using antibodies as the detection elements, the concentration range of detection was greatly reduced. The use of the Ab-HMS conjugates increased the sensitivity and specificity of the immunosensor. This electrochemical immunosensor had good selectivity and a fast detection time (20 min) with a sensitive detection limit of 11 CFU mL<sup>-1</sup> and a concentration range of 10 to 2 × 10<sup>3</sup> CFU mL<sup>-1</sup> by using DPV detection. At the same time, when the EIS is tested under the same conditions, the same trend as the DPV is obtained, and there is a good linear relationship between the resistance difference and the bacterial concentration ( $R^2 = 0.9720$ ), which proves that the sensor has a reliable application prospect. The covalent bonding between the carrier material and the antibody utilizes both preparation time and improved sensor stability. The sensor device can be stabilized for 15 days. This study has the potential to quantify low concentrations of foodborne bacteria with a high sensitivity and selectivity in the food and environmental safety field.

## Conflicts of interest

The authors declare no conflict of interest.

## Acknowledgements

This work was supported by National Nature Science Foundation of China [Grant No. 31572566 and 31872525 to X. D. N], the Key Program of Jilin Province [Grant No. 20180201044NY], and Jilin Educational Committee [Grant No. 3D518L714071].

## References

- H. Wang, R. Luo, Y. Chen, Q. Si and X. Niu, *J. Electron. Mater.*, 2018, **47**, 4124–4135.
- C. Letertre, S. Perelle, F. Dilasser and P. Fach, *Mol. Cell. Probes*, 2003, **17**, 139–147.
- X. Meng, G. Yang, F. Li, T. Liang, W. Lai and H. Xu, *ACS Appl. Mater. Interfaces*, 2017, **9**, 21464–21472.
- H. Yang, X. Ma, X. Zhang, Y. Wang and W. Zhang, *Eur. Food Res. Technol.*, 2011, **232**, 769–776.
- S. Ranjbar and S. Shahrokhian, *Bioelectrochemistry*, 2018, **123**, 70–76.
- S. Wang, W. Deng, L. Yang, Y. Tan, Q. Xie and S. Yao, *ACS Appl. Mater. Interfaces*, 2017, **9**, 24440–24445.
- X. Xie, L. Rieth, S. Merugu, P. Tathireddy and F. Solzbacher, *Appl. Phys. Lett.*, 2012, **101**, 93702.
- R. Chauhan, J. Singh, P. R. Solanki, T. Manaka, M. Iwamoto, T. Basu and B. D. Malhotra, *Sensor. Actuator. B Chem.*, 2016, **222**, 804–814.
- J. Singh, A. Roychoudhury, M. Srivastava, P. Solanki, D.-W. Lee, S. Hee Lee and B. Malhotra, *J. Mater. Chem. B*, 2013, **1**, 4493–4503.
- M. Rubab, H. M. Shahbaz, A. N. Olaimat and D.-H. Oh, *Biosens. Bioelectron.*, 2018, **105**, 49–57.
- P. R. Solanki, J. Singh, B. Rupavali, S. Tiwari and B. D. Malhotra, *Mater. Sci. Eng. C*, 2017, **70**, 564–571.
- R. Chauhan, J. Singh, P. R. Solanki, T. Basu, R. O'Kennedy and B. D. Malhotra, *Biochem. Eng. J.*, 2015, **103**, 103–113.
- T. Kaneko, F. Nagata, S. Kugimiya and K. Kato, *Ceram. Int.*, 2018, **44**, 20581–20585.
- B. Yang, Y. Chen and J. Shi, *Adv. Healthc. Mater.*, 2018, **7**, 1800268–1800278.
- Y. Zhang, X. Liu and J. Huang, *ACS Appl. Mater. Interfaces*, 2011, **3**, 3272–3275.
- T.-X. Fan, S.-K. Chow and D. Zhang, *Prog. Mater. Sci.*, 2009, **54**, 542–659.
- I. Cho, K. Kang, D. Yang, J. Yun and I. Park, *ACS Appl. Mater. Interfaces*, 2017, **9**, 27111–27119.
- E. Dujardin and S. Mann, *Adv. Eng. Mater.*, 2002, **4**, 461–474.
- J. Ma, H. Fan, X. Ren, C. Wang, H. Tian, G. Dong and W. Wang, *ACS Sustainable Chem. Eng.*, 2019, **7**, 147–155.
- X. Lin, X. Wang, L. Li, M. Yan and Y. Tian, *ACS Sustainable Chem. Eng.*, 2017, **5**, 9709–9717.
- Q. Fu, F. Ansari, Q. Zhou and L. A. Berglund, *ACS Nano*, 2018, **12**, 2222–2230.
- L. A. Berglund and I. Burgert, *Adv. Mater.*, 2018, **30**, 1–15.
- Y. Ding, J. Yang, C. R. Tolle and Z. Zhu, *ACS Appl. Mater. Interfaces*, 2018, **10**, 16077–16086.
- J. G. Kim, M. C. Cha, J. Lee, T. Choi and J. Y. Chang, *ACS Appl. Mater. Interfaces*, 2017, **9**, 38081–38088.
- J. Bhardwaj, S. Devarakonda, S. Kumar and J. Jang, *Sensor. Actuator. B Chem.*, 2017, **253**, 115–123.
- A. Abbaspour, F. Norouz-Sarvestani, A. Noori and N. Soltani, *Biosens. Bioelectron.*, 2015, **68**, 149–155.
- V. Escamilla-Gómez, S. Campuzano, M. Pedrero and J. M. Pingarrón, *Anal. Bioanal. Chem.*, 2008, **391**, 837–845.
- H. Cao, D.-P. Yang, D. Ye, X. Zhang, X. Fang, S. Zhang, B. Liu and J. Kong, *Biosens. Bioelectron.*, 2015, **68**, 329–335.
- S.-L. Zhong, J. Zhuang, D.-P. Yang and D. Tang, *Biosens. Bioelectron.*, 2017, **96**, 26–32.
- C. Hu, D.-P. Yang, K. Xu, H. Cao, B. Wu, D. Cui and N. Jia, *Anal. Chem.*, 2012, **84**, 10324–10331.
- G. O. Park, J. Yoon, S. B. Park, Z. Li, Y. S. Choi, W.-S. Yoon, H. Kim and J. M. Kim, *Small*, 2018, **14**, 1702985.
- J. Zong, Y. S. Zhang, Y. Zhu, Y. Zhao, W. Zhang and Y. Zhu, *Sensor. Actuator. B Chem.*, 2018, **271**, 311–320.
- P. Verma, K. Yuan, Y. Kuwahara, K. Mori and H. Yamashita, *Appl. Catal. B Environ.*, 2018, **223**, 10–15.
- D. Breznan, D. D. Das, C. MacKinnon-Roy, S. Bernatchez, A. Sayari, M. Hill, R. Vincent and P. Kumarathanan, *ACS Nano*, 2018, **12**, 12062–12079.
- W. Shan, D. Zhang, X. Wang, D. Wang, Z. Xing, Y. Xiong, Y. Fan and Y. Yang, *Microporous Mesoporous Mater.*, 2019, **278**, 44–53.
- D. M. Eby, K. Artyushkova, A. K. Paravastu and G. R. Johnson, *J. Mater. Chem.*, 2012, **22**, 9875–9883.



- 37 D. M. Eby, K. Artyushkova, A. K. Paravastu and G. R. Johnson, *J. Mater. Chem.*, 2012, **22**, 9875–9883.
- 38 X. Meng, G. Yang, F. Li, T. Liang, W. Lai and H. Xu, *ACS Appl. Mater. Interfaces*, 2017, **9**, 21464–21472.
- 39 S. Zhu, D. Zhang, Z. Li, H. Furukawa and Z. Chen, *Langmuir*, 2008, **24**, 6292–6299.
- 40 R. Jain, N. Jadon and A. Pawaiya, *Trac. Trends Anal. Chem.*, 2017, **97**, 363–373.
- 41 N. Bhardwaj, S. K. Bhardwaj, J. Mehta, K.-H. Kim and A. Deep, *ACS Appl. Mater. Interfaces*, 2017, **9**, 33589–33598.
- 42 A. C. Ward, A. J. Hannah, S. L. Kendrick, N. P. Tucker, G. MacGregor and P. Connolly, *Biosens. Bioelectron.*, 2018, **110**, 65–70.
- 43 W. Hertl, *Bioelectrochem. Bioenerg.*, 1987, **17**, 89–100.
- 44 J. G. Swoboda, J. Campbell, T. C. Meredith and S. Walker, *ChemBioChem*, 2010, **11**, 35–45.
- 45 S. Kumar, J. G. Sharma, S. Maji and B. D. Malhotra, *J. Phys.: Conf. Ser.*, 2016, **6**, 10.
- 46 J. Okuno, K. Maehashi, K. Kerman, Y. Takamura, K. Matsumoto and E. Tamiya, *Biosens. Bioelectron.*, 2007, **22**, 2377–2381.
- 47 G. A. R. Y. Suaifan, S. Alhogail and M. Zourob, *Biosens. Bioelectron.*, 2017, **90**, 230–237.
- 48 H. Yue, Y. Zhou, P. Wang, X. Wang, Z. Wang, L. Wang and Z. Fu, *Talanta*, 2016, **153**, 401–406.
- 49 X. Liu, M. Marrakchi, D. Xu, H. Dong and S. Andreescu, *Biosens. Bioelectron.*, 2016, **80**, 9–16.

